

BULK ANTIBODIES
for *in vivo*
RESEARCH

α-CD4 **α-CD8** **α-CD25** **α-NK1.1** **α-Ly6G**

Discover More

BioCell



Crystal Structure of the Labile Complex of IL-24 with the Extracellular Domains of IL-22R1 and IL-20R2

This information is current as of January 24, 2019.

Jacek Lubkowski, Cem Sonmez, Sergey V. Smirnov, Andriy Anishkin, Sergei V. Kotenko and Alexander Wlodawer

J Immunol 2018; 201:2082-2093; Prepublished online 15 August 2018;

doi: 10.4049/jimmunol.1800726

<http://www.jimmunol.org/content/201/7/2082>

References This article **cites 41 articles**, 11 of which you can access for free at: <http://www.jimmunol.org/content/201/7/2082.full#ref-list-1>

Why *The JI*? Submit online.

- **Rapid Reviews! 30 days*** from submission to initial decision
- **No Triage!** Every submission reviewed by practicing scientists
- **Fast Publication!** 4 weeks from acceptance to publication

**average*

Subscription Information about subscribing to *The Journal of Immunology* is online at: <http://jimmunol.org/subscription>

Permissions Submit copyright permission requests at: <http://www.aai.org/About/Publications/JI/copyright.html>

Email Alerts Receive free email-alerts when new articles cite this article. Sign up at: <http://jimmunol.org/alerts>



Crystal Structure of the Labile Complex of IL-24 with the Extracellular Domains of IL-22R1 and IL-20R2

Jacek Lubkowski,* Cem Sonmez,* Sergey V. Smirnov,[†] Andriy Anishkin,[‡] Sergei V. Kotenko,[†] and Alexander Wlodawer*

Crystal structure of the ternary complex of human IL-24 with two receptors, IL-22R1 and IL-20R2, has been determined at 2.15 Å resolution. A crystallizable complex was created by a novel approach involving fusing the ligand with a flexible linker to the presumed low-affinity receptor, and coexpression of this construct in *Drosophila* S2 cells together with the presumed high-affinity receptor. This approach, which may be generally applicable to other multiprotein complexes with low-affinity components, was necessitated by the instability of IL-24 expressed by itself in either bacteria or insect cells. Although IL-24 expressed in *Escherichia coli* was unstable and precipitated almost immediately upon its refolding and purification, a small fraction of IL-24 remaining in the folded state was shown to be active in a cell-based assay. In the crystal structure presented here, we found that two cysteine residues in IL-24 do not form a predicted disulfide bond. Lack of structural restraint by disulfides, present in other related cytokines, is most likely reason for the low stability of IL-24. Although the contact area between IL-24 and IL-22R1 is larger than between the cytokine and IL-20R2, calculations show the latter interaction to be slightly more stable, suggesting that the shared receptor (IL-20R2) might be the higher-affinity receptor. *The Journal of Immunology*, 2018, 201: 2082–2093.

Human IL-24 was originally described as a product of melanoma differentiation associated gene *mda-7* (1). IL-24 displays a variety of physiological activities, among which is an ability to suppress proliferation of several cancer cell lines (2). Clinical trials utilizing IL-24 as a putative anticancer agent have been taking place for a number of years (3–5), although this cytokine is not yet approved as a drug.

The most widely recognized property of cytokines is their affinity for specific receptors capable of forming heterodimeric transmembrane complexes, the cytoplasmic domains of which are constitutively associated with JAK kinases. Binding of cytokines to the extracellular domains of heterodimeric receptors triggers a sequence of phosphorylation events constituting the initial steps of the JAK-STAT signaling pathway. Based on the signature sequences within extracellular domains, cytokine receptors are classified into two classes, 1 and 2.

IL-24 belongs to the family of cytokines interacting with class 2 cytokine receptors. This family additionally includes five other ILs (IL-10, IL-19, IL-20, IL-22, and IL-26), as well as IFNs from three different subfamilies, α/β , γ , and λ . The IL subset is often referred to as the IL-10 family (6). Three of these ILs, IL-19, IL-20, and IL-24, designated IL-20 subfamily cytokines (IL-20SFCs), signal through receptor complexes that share the common chain, IL-20R2. Additionally, IL-20 and IL-24 share with IL-22 another receptor chain, IL-22R1, although the latter cytokine utilizes IL-10R2 as its second receptor.

The open reading frame of IL-24 encodes a polypeptide chain composed of 206 aa residues; however, excision of the signal peptide leads to the mature form consisting of 155 residues. Interestingly, the signal peptide in IL-24 (51 aa) is twice as long as in other related human cytokines. Whereas the predicted molecular mass of IL-24 monomer is 18.3 kDa, well-established *N*-glycosylation of up to three sites in mammalian cells (7) leads to expression of several isoforms, with molecular mass ranging from 18.3 kDa up to 35 kDa (8). It was previously suggested that *N*-glycosylation of IL-24 is dispensable for induction of tumor cell apoptosis and related activities (9). Other data indicated that partial *N*-linked glycosylation and one disulfide bond are required for solubility and bioavailability of IL-24 and attempts to produce biologically active IL-24 in bacteria were unsuccessful (7). Although production of active IL-24 and its mutant in *Escherichia coli* has been reported more recently (10, 11), there is no evidence that the amounts of stable cytokine sufficient for structural studies have ever been obtained in bacteria.

IL-24 forms signaling complexes with two different receptor pairs, IL-20R1/IL-20R2 and IL-22R1/IL-20R2, which it shares with the other IL-20SFCs and IL-22. These complexes were defined as type I (with the IL-20R1/IL-20R2 pair of receptors) and type II (IL-22R1/IL-20R2) (12, 13). For both types of complexes, the signaling events are accomplished by the activation of the Tyk2/Jak1 → STAT1/STAT3 pathway. Several structures of these cytokines, either alone or bound to their receptors, are available. Crystal structures of free IL-19 (14) and IL-22 (15, 16) have been previously determined. Crystal structures are also available for the

*Macromolecular Crystallography Laboratory, Center for Cancer Research, National Cancer Institute, Frederick, MD 21702; [†]Department of Microbiology, Biochemistry and Molecular Genetics, Center for Immunity and Inflammation, Rutgers Cancer Institute of New Jersey at University Hospital, New Jersey Medical School, Rutgers University, Newark, NJ 07103; and [‡]Biology Department, University of Maryland, College Park, MD 20742

ORCID: 0000-0002-6071-641X (C.S.).

Received for publication May 23, 2018. Accepted for publication July 11, 2018.

This work was supported by the Intramural Research Program of the National Institutes of Health (NIH), National Cancer Institute Center for Cancer Research to J.L. and A.W. and by NIH Grant R01 AI51139 to S.V.K. Use of the Advanced Photon Source was supported by the Basic Energy Sciences program of the U.S. Department of Energy, Office of Science under Contract W-31-109-Eng-38.

The sequences presented in this article have been submitted to the Protein Data Bank (<http://www.rcsb.org>) under accession number 6df3.

Address correspondence and reprint requests to Dr. Jacek Lubkowski, National Cancer Institute, 536 Boyles Street, Frederick, MD 21702. E-mail address: lubkowsj@mail.nih.gov

Abbreviations used in this article: CM, complete medium; IB, inclusion body; ID, identifier; IL-20SFC, IL-20 subfamily cytokine; IL-24_{w.t.}, wild type IL-24; IPTG, isopropyl- β -D-1-thiogalactopyranoside; NEB, New England Biolabs; PDB, Protein Data Bank; RH, high-affinity receptor; RL, low-affinity receptor; RMSD, root mean square deviation; sIL-20R1, soluble IL-20R1.

Copyright © 2018 by The American Association of Immunologists, Inc. 0022-1767/18/\$35.00

binary complexes of IL-22 with its high-affinity receptor (RH) chain IL-22R1 (17, 18). Additionally, the structure of the ternary complex IL-20/IL-20R1/IL-20R2 has also been determined (13). Thus the structures of all receptors used by IL-24 are already known (but in complexes with other family members). No crystal structure of IL-24, either free or in the form of a ligand/receptor complex, has been published to date, although a model based on the close homology with IL-19, IL-20, and IL-22 has been proposed (19). In this article, we present several approaches to expressing IL-24 and its receptors and evaluating the biological activity of the cytokine. Furthermore, we describe the crystal structure of IL-24 in the type II ternary complex (IL-24/IL-22R1/IL-20R2) and compare it with the structures of closely related cytokines.

Materials and Methods

Construction of plasmids and expression of wild type IL-24 in *E. coli*

A synthetic gene, codon-optimized for *E. coli* expression and encoding the mature wild type IL-24 (IL-24_{wt}; aa 52–206) and a cleavable N-terminal affinity tag, “HHHHHHENLYFQ” (the underlined fragment corresponds to the TEV protease recognition sequence), was purchased from GeneScript. The gene was cloned into the Gateway System (Thermo Fisher Scientific). The expression vector pDEST 14 (Thermo Fisher Scientific) was used for transforming BL21(DE3) pLysS cells (Agilent Technologies), and expression was attempted under various regimens of temperature, time, and induction point. The expression experiments invariably resulted in production of an insoluble product, identified as IL-24 by Western analysis using both Penta-His (Qiagen) and anti-IL-24 (R&D Systems) Abs. Subsequently, the synthetic gene of IL-24_{wt} was cloned in frame into three additional vectors, pRSET A (Thermo Fisher Scientific), pET32a(+) (EMD Millipore), and pMAL C5X (New England Biolabs [NEB]), resulting in the following constructs: MRGS–(His)₆–“Xpress-epitope-tag”–“enterokinase-cleavage site”–IL-24_{wt}–STP, Thioredoxin–(His)₆–“TEV cleavage site”–IL-24_{wt}–STP, and “Maltose binding protein”–(His)₆–“TEV cleavage site”–IL-24_{wt}–STP. These constructs were used for transformation of the BL21(DE3) pLysS cells. The latter two constructs were aimed at production of IL-24_{wt} N-terminally fused to cleavable protein partners, with an expectation of improved solubility and/or folding supported by disulfide formation, compared with expression of the unfused cytokine. The correctness of these constructs was confirmed by sequencing (Macrogen). For each of the three constructs, expression experiments were conducted at two temperatures, 37 and 18°C. In the case of the construct based on pRSET A, IL-24_{wt} was expressed in an insoluble form with a lower yield compared with that obtained from the Gateway vector. Both fusion proteins were also accumulating mostly in the inclusion bodies (IBs), with only a small fraction remaining in the soluble form. However, following cleavage of fusion partners with TEV protease, the released IL-24_{wt} rapidly precipitated.

Because refolding became an unavoidable step for a preparation of soluble IL-24_{wt}, a new expression vector encoding Met-IL-24_{wt} [i.e., lacking the (His)₆–ENLYFQ sequence] was generated with a QuikChange protocol using the original Gateway-based construct and used for transformation of BL21(DE3) pLysS cells. Cells were grown at 37°C in the lysogeny broth medium supplemented with ampicillin (100 µg/ml). After cell density reached a midlog phase (OD₅₉₅ 0.5 / 0.7), expression was induced with the isopropyl-β-D-1-thiogalactopyranoside (IPTG) supplied at the concentration of 1 mM. Growth of the cell culture continued at 37°C for an additional 3–4 h, reaching OD₅₉₅ 3.5–4.5. The cell pellet was collected by a centrifugation at 6000 × g for 20 min and was subsequently suspended in 150 ml of the lysis buffer (50 mM Tris, pH 8, 150 mM NaCl) supplemented with 10 mM MgCl₂, 10 mM CaCl₂, 20 µg/ml DNase I (Roche), 20 µg/ml RNase A (Thermo Fisher Scientific), and the complete Protease Inhibitor Cocktail (Roche) and frozen at –80°C for further use.

Purification and refolding of insoluble IL-24_{wt}

The suspension of *E. coli* cells expressing insoluble IL-24_{wt} was thawed on ice and subjected to cell lysis using the APV-1000 homogenizer (Invensys APV Products, Albertslund, Denmark) operating at 70 MPa. Insoluble fractions (IBs) were collected by centrifugation at 35,000 × g for 30 min. IBs were washed twice with 100 ml of 50 mM Tris (pH 8) with 20 mM 2-ME, 1 mM EDTA, and 2% Triton X-100, followed by two washes with the same buffer but without Triton X-100. Subsequently, IBs were solubilized in 120 ml of the denaturing buffer (6 M guanidinium chloride, 50 mM Tris,

pH 8, 20 mM DTT, 1 mM EDTA). Insoluble residue was removed by centrifugation (35,000 × g for 30 min). The cleared solution was gradually diluted with 40 ml of buffer A consisting of 10% (v/v) solution of acetonitrile, supplemented with 0.1% trifluoroacetic acid—further dilution led to precipitation of the protein. The diluted solution was applied onto the 100 × 7.5 mm PEEK column, custom-packed with the POROS R2 20 µm reverse-phase resin (Thermo Fisher Scientific), and washed extensively with buffer A. Protein was eluted at a flow rate 10 ml/min with a linear gradient (10–35% v/v) of acetonitrile. Fractions containing IL-24 (identified by SDS-PAGE, NaDodSO₄-PAGE) were pooled and lyophilized. The molecular mass, measured by electrospray ionization mass spectroscopy, was 18,268.3 Da, which is in good agreement with the theoretical value of 18,268.1 Da.

About 50 mg of lyophilized sample was dissolved in 100 ml of a buffer containing 6 M guanidinium chloride, 0.1 M Tris (pH 8), 0.5 M arginine hydrochloride, 5% (v/v) glycerol, and 1 mM EDTA, as well as 5 mM reduced and 0.5 mM oxidized glutathione. In addition to gentle rocking of the sample vial, solubilization was enhanced by several short bursts of sonication on ice. The resulting sample was diluted 20-fold with a solution containing 0.1 M Tris (pH 8), 0.5 M arginine hydrochloride, 0.5 M sodium chloride, 5% (v/v) glycerol, 1 mM EDTA, 5 mM reduced, and 0.5 mM oxidized glutathione and stirred for 48 h at 4°C. Subsequently, the solution containing soluble IL-24 was filtered through a 0.22 µm polyethersulfone membrane and concentrated using the Amicon YM10 membrane fixed in a compatible stirred cell (EMD Millipore), to the final volume of 100 ml. That solution was dialyzed overnight using a 45 mm/MWCO 3500 membrane (Spectrum Labs.) against 3.5 l of buffer B containing 0.1 M Tris (pH 8), 0.5 M sodium chloride, and 5% (v/v) glycerol. Dialysis resulted in substantial precipitation of misfolded IL-24_{wt}, which was removed by centrifugation. A cleared solution (~110 ml) of refolded IL-24 was concentrated 20-fold using a stirred cell with an Amicon YM10 membrane and applied onto a HiPrep 16/60 Superdex 200 HR column (GE Healthcare Life Sciences) equilibrated with buffer B. Fractions containing the recombinant protein were identified using SDS-PAGE, pooled, and concentrated using the Amicon YM10 membrane. The final sample of IL-24 was judged to be >95% pure by SDS-PAGE. The molecular mass was 18,266.6 Da, as compared with the theoretical 18,266.2 Da.

Construction of plasmids for expression in *Drosophila* S2 cells

DNA sequences encoding proteins of interest were amplified from the cDNA samples purchased from OriGene (www.origene.com). They included IL-24 (cat. no. RC216502), IL-20R1 (cat. no. RC238599), IL-20R2 (cat. no. RC213197), and IL-22R1 (cat. no. RC206447). Plasmids used for the expression of proteins in *Drosophila* S2 Schneider cells were generated with an aid of the commercial pMT/BiP/V5-His A vector (Thermo Fisher Scientific), utilizing the BglII and AgeI sites. The DNA fragments (inserts) encoding extracellular regions of the mature IL-20R1 (aa 30–250, Q9UHF4/UniProt; NM_001278722.1/GenBank, residue numbers correspond to native translated genes that include signal sequences), IL-20R2 (aa 30–233, Q6UXL0/UniProt; NM_144717.3/GenBank), IL-22R1 (aa 15–228, Q8N6P7/UniProt; NM_021258.3/GenBank), and the sequence corresponding to mature IL-24 (aa 52–206, Q13007/UniProt; NM_001185156.1/GenBank) were PCR amplified (using *PfuUltra* II Hotstart PCR Master Mix; Agilent Technologies) in the presence of appropriately designed synthetic primers (Integrated DNA Technologies) and gel purified after sequential digest with BglII and AgeI (NEB). The native pMT/BiP/V5-His A vector was subjected to a similar protocol resulting in BglII-vector-AgeI. After ligations (using Quick Ligation kit; NEB) of inserts with BglII-vector-AgeI, plasmids were transformed in *E. coli* DH5α and plated on lysogeny broth substrate with ampicillin (100 µg/ml), and individual clones were selected for preparation and sequencing (Macrogen) of plasmids used for expression of soluble IL-20R1 (sIL-20R1), sIL-20R2, sIL-22R1, and IL-24.

All these wild type variants carry multiple potential *N*-glycosylation sites, the presence of which could be detrimental for crystallization. Therefore, several constructs encoding *N*-deglycosylated variants of the abovementioned proteins were also generated by mutating appropriate codons (Asn→Gln). This task was accomplished with the aid of the QuikChange strategy (see www.genomics.agilent.com/files/Manual/200523.pdf; Agilent Technologies). The resulting plasmids were IL-24_{Q85Q99Q126} (asparagines 85, 99, and 126 mutated to glutamines), IL-20R2_{Q40Q134}, and IL-20R1_{K111RK113R}. IL-24_{Q85Q99Q126} represents the fully *N*-deglycosylated variant, whereas mutations introduced to the genes encoding soluble fragments of the IL-20Rs followed the earlier suggestions (13). In addition, plasmids encoding the sequences of three fusion proteins were also constructed, based on the native pMT/BiP/V5-His A vector. They included sIL-20RA-linker-IL-24_{Q85Q99Q126}, sIL-20RB-linker-IL-24_{Q85Q99Q126}, and sIL-22RA-linker-IL-24_{Q85Q99Q126}, where the linker sequence GGGGSETVRFQSGGGSEGGSE

included the recognition sequence ETVRFQS of the TVMV protease. To generate each of the fusion inserts flanked by the BglIII and AgeI restriction sites (see above), fragments for each fusion partner were first PCR amplified with pairs of synthetic DNA primers (Integrated DNA Technologies). Whereas the upstream primers in each of the two fragments were the same as those used in earlier cloning experiments and encoded appropriate restriction sites, the downstream primers were largely complementary and, when assembled, encoded the linker sequence. Pairs of PCR-amplified fragments were assembled by PCR reaction into complete fusion inserts and treated subsequently as described above. All plasmids aimed at the protein expression in *Drosophila* S2 Schneider cells encoded open reading frames following a common structure, BiP-RS-insert-TG-His6-STP, in which BiP encodes signal sequence, RS and TG are cloning artifacts (representing BglIII and AgeI restriction sites, respectively), insert corresponds to the protein of interest, His6 encodes the His₆ sequence of the affinity tag, and STP is the termination signal. In addition, the TEV protease recognition sequence ENLYFQG was embedded at the 3' terminus of the insert in constructs encoding fusion proteins.

Expression experiments in *Drosophila* S2 cells and protein purification

Plasmids encoding the components of the IL-24 signaling complex were used for transfection of *Drosophila* S2 Schneider cells (cat. no. R690-07; Thermo Fisher Scientific) to establish stably transfected cell lines. Briefly, a culture (~5 ml) of high-viability S2 cells in the SFX Insect media (Thomas Scientific) supplemented with 10% (v/v) heat-inactivated FBS (Thomas Scientific) was used to inoculate several small cultures (in six-well plate, ~2.4 ml/well per transection) in fresh complete medium (CM) (SFX Insect with FBS) to the cells density ~10⁶ cells/ml. Cells were left to adhere for ~4–6 h at 28°C. The transfection protocol used the Effectene Transfection Reagent (cat. no. 301425; Qiagen) and followed manufacturer recommendations. Cells were always cotransfected with a mixture of an expression vector and pCoBlast (Thermo Fisher Scientific) at an approximate molar ratio 1:19, with the latter vector providing blasticidin resistance. When the S2 cells were cotransfected with several expression vectors, different concentration ratios of these vectors were tested, whereas the concentration of pCoBlast was usually 19 times higher than the combined concentration of expression vectors. After 2–4 d, when the cell viability was ascertained (usually by visual inspection), most of the medium was replaced with fresh CM supplemented with blasticidin S (cat. no. A1113902; Thermo Fisher Scientific) at the concentration 10–20 µg/ml. After this step, every 2–4 d, cells were pelleted by centrifugation (100–500 × g, 5–8 min.) and resuspended in fresh CM supplemented with gradually increased concentrations of blasticidin S (maximum concentration 25–30 µg/ml). After several passages, the volumes of cell cultures were expanded. The selection process was usually complete after 4 wk. Subsequently, small aliquots of stably transfected cells were frozen following a standard protocol (see the *Drosophila* Expression System manual, https://assets.thermofisher.com/TFS-Assets/LSG/manuals/des_man.pdf), whereas part of each cell culture was subjected to expression trials (appropriate protocols are described in the *Drosophila* Expression System manual). At this stage, production and identities of proteins were confirmed by the SDS-PAGE and Western analysis using specific Abs.

Expression utilizing the pMT/BiP/His A vector was induced with Cu²⁺ ions, and proteins were secreted to the media. For large-scale expression, transfected cells were cultured in T-75 flasks in CM supplemented with blasticidin S until the culture volume reached 20–30 ml and density reached ~5 × 10⁶ cells/ml. At this stage, cells were harvested by centrifugation (100–500 × g, 5–8 min), resuspended in fresh serum-free SFX Insect medium to assure the density >2 × 10⁶ cells/ml, and transferred to an appropriate shaker flask (assuring good aeration). Flasks were placed in the incubated shaker and agitated at 105–125 rpm. Cell density and viability were monitored daily, and gradually, the cultures were expanded to the final volumes of 2 l. Approximately 12 h prior to induction, cells were harvested and resuspended in fresh SFX Insect medium. Protein expressions were induced with 100 mM copper sulfate solution to the final concentration of Cu²⁺ ions between 500 and 750 µM. Expression usually continued for additional 4–5 d, with cell growth and viability monitored daily. A medium with the expressed protein product was harvested by centrifugation (6000 × g for 30 min), cleared using 0.22 µm filters, and immediately subjected to a purification procedure.

A typical purification protocol consisted of three steps. First, protein-containing media were applied onto a 5 ml HisTrap Excel column (cat. no. 17371206; GE Healthcare Life Sciences). Extensive wash with buffer A containing 500 mM NaCl and 20 mM sodium phosphate (pH 7.4) was followed by wash with buffer A supplemented with 30 mM imidazole. Protein was eluted with buffer A supplemented with 500 mM imidazole.

At this stage, a majority of the protein was isolated, and the volume of a protein sample was usually between 20 and 50 ml; however, the purity of the preparation assessed by SDS-PAGE was inferior compared with typical Ni-affinity purification. Therefore, in the next step, protein solution was either diluted 7–10 times with buffer A or dialyzed against this buffer overnight (to lower the concentration of imidazole) and applied onto a second Ni-affinity column, 5 ml HisTrap HP (cat. no. 17-5247-01; GE Healthcare Life Sciences). The purification protocol mirrored very closely the one described earlier except that elution was usually accomplished with 250–300 mM imidazole. After concentrating the fractions containing a target protein, the sample was applied onto the size exclusion column Superdex 75 Increase (cat. no. 29148721; GE Healthcare Life Sciences) and equilibrated/eluted in the final buffer containing 50 mM Tris (pH 7.5) and 200 mM NaCl. After assuring purity, protein preparations were concentrated, frozen, and stored at –80°C for further use.

Mass spectroscopy analysis

All measurements of molecular mass referred to in this manuscript were performed by means of the MALDI-TOF mass spectroscopy using Agilent 6100 series single quadrupole LC/Mass Selective Detector (Agilent Technologies).

Western blot analysis

SDS-PAGE analyses were performed using Novex NuPAGE SDS-PAGE gel system on NuPAGE Bis-Tris precast gels (Thermo Fisher Scientific). Proteins were transferred from gels to nitrocellulose membranes with the iBlot Dry Blotting System (Thermo Fisher Scientific). The following Abs were used during analyses: anti-IL-24, cat. no. AF1965; anti-IL-20R1, cat. no. AF1176; anti-IL-20R2, cat. no. AF1788; and anti-IL-22R1, cat. no. AF2770 (all from R&D Systems) as well as anti-Penta-His-tag, cat. no. 34660 (Qiagen).

EMSA

Hamster cells expressing chimeric human IL-20R1/γR1 and intact human IL-20R2 were collected by trypsinization, aliquoted into tubes (10⁵ cells/200 µl), and treated with various concentrations of IL-24 samples for 15 min and used in EMSAs to detect STAT1 activation with the γ-activated sequence probe as described (20, 21). EMSAs were performed with a 22 bp sequence containing a Stat1α binding site corresponding to the γ-activated sequence element in the promoter region of the human IRF-1 gene (5'-GATCGATTTCCTCCCGAAATCATG-3') (22). Two oligonucleotides, 5'-GATCGATTTCCTCCCGAAAT-3' and 5'-CATGATTTCGGGA-AATC-3', were annealed by incubation for 10 min at 65°C, 10 min at 37°C, and 10 min at 22°C and labeled with [³²P]dATP by filling-in with the Klenow fragment of DNA polymerase I in the presence of the other three dNTPs. Whole-cell extracts were prepared as followed. Untreated or IL-24-treated cells were precipitated by centrifugation at 3000 × g for 1 min, washed with 1.0 ml of cold PBS, pelleted again, and resuspended in 50 µl of lysis buffer (10% glycerol, 50 mM Tris-HCl, pH 8, 0.5% Nonidet P-40, 150 mM NaCl, 0.1 mM EDTA, 1 mM DTT, 0.2 mM PMSF, 1 mM Na₃VO₄, 3 µg/ml aprotinin, 1 µg/ml pepstatin, and 1 µg/ml leupeptin). After 30 min on ice, the extracts were centrifuged for 5 min at full speed in a microcentrifuge, and the supernatant was recovered and used directly for EMSAs or stored at –80°C until use. EMSA reactions contained 2.5 µl nuclear extract, 1 ng ³²P-labeled probe (sp. act. 10⁹ cpm/µg), BSA (24 µg/ml), poly(dI:dC) (160 µg/ml), 20 mM HEPES (pH 7.9), 1 mM MgCl₂, 4.0% Ficoll (Sigma-Aldrich), 40 mM KCl, 0.1 mM EGTA, and 0.5 mM DTT in a total volume of 12.5 µl. Incubations were performed at 22°C for 20 min, then 4 µl of the reaction mixture were electrophoresed at 400 V for 3–4 h at 4°C on a 20 × 20 cm² 5% polyacrylamide (19:1 acrylamide/bisacrylamide) gel. The dried gel was exposed to Kodak XAR-5 film with intensifying screens for 12 h at –80°C.

Crystallization, data collection, and structure solution

Crystals of the ternary complex were grown by vapor diffusion in hanging droplets formed by mixing equal volumes of the protein solution (8 mg/ml in 200 mM NaCl and 50 mM HEPES, pH 7) and the reservoir solution (21% w/v MePEG2000, 50 mM Tris, pH 8.5, 50 mM trimethylamine *N*-oxide dihydrate). Crystals grew within 3–5 d. For data collection, crystals were cryoprotected by brief transfer to the reservoir solution enriched with 10% (v/v) of glycerol and frozen in liquid nitrogen. X-ray data were collected from one crystal on beamline 22-ID at the Advanced Photon Source, Argonne National Laboratory (Argonne, IL). All diffraction experiments were conducted at –173°C. The experimental images were processed and scaled using the program *HKL3000* (23). Details of experimental data collection and processing statistics are presented in Table I. The structure

was solved by molecular replacement with the program *PHASER* (24) using the coordinates of the IL-20/IL-20R1/IL-20R2 ternary complex [Protein Data Bank (PDB) identifier (ID): 4doh (13)] as the search model. Data extending to 2.5 Å were used for molecular replacement, yielding *Z*-score of 42.5 and the log-likelihood gain of 10,796. Subsequently, using complete data set within resolution ranges 30–2.15 Å, the solution was rebuilt, including conversion to the correct amino acid sequence, with the aid of the programs *PHENIX* (25) and *MR Rosetta* (26), with final refinement using *Refmac5* (27). In addition to the sequence conversion, a total of 506 aa residues and 172 pseudo-water atoms were modeled in the electron density. At this stage, the values of the R_{work} and R_{free} were 0.265 and 0.325, respectively, and the stereochemistry of the model was mostly correct. The final steps of model improvement included a series of manual corrections, refinement, and monitoring aided by the programs *Coot* (28), *Refmac5* (27), and *Molprobity* (29). The final model is characterized by R_{work} and R_{free} values 0.183 and 0.225, respectively, with acceptable stereochemistry. Detailed characteristics of the final model are shown in Table II.

Evaluation of the interfaces between the cytokine and the receptors

The extent and the energy contribution of the interfaces between IL-24 and the receptors were evaluated with the web servers PDBePISA (<http://www.ebi.ac.uk/pdbe/pisa/>) and CCharPPI (<https://life.bsc.es/pid/ccharppi>). Whereas PDBePISA directly calculates the buried surfaces and estimates the binding energies due to interatomic interactions, CCharPPI provides access to the scores of 108 quantitative descriptors of protein–protein interactions developed by different research groups. The descriptors range from particular contributions to binding energy (e.g., van der Waals, electrostatics, hydrogen bonds, solvation energies) to the net energy of the whole interface, based on either on empirical functions, geometry of the contacts, or various statistical estimators. To estimate the free energy of binding based on descriptor scores, we have used as a reference the Affinity benchmark dataset with the same scores precalculated for 144 proteins with experimentally measured binding energy (30). For every available descriptor, we have calculated a linear fit (least squares method) of the experimental binding energy versus the descriptor score. Out of 108 descriptors available on the CCharPPI server, we were able to match and fit 106 using the database. Although for any of the individual descriptors, the Pearson correlation coefficient with the energy was estimated to be below 40%, the large number of estimates and the agreement among the predicted energy values for different approaches bring reasonable confidence in the results.

Accession numbers

The coordinates and structure factors have been deposited in the PDB (<http://www.rcsb.org>, accession code 6df3).

Results

E. coli-derived IL-24 is unstable but signals through its cognate receptors

Because some IL-10–related cytokines have been previously prepared using *E. coli* bacterial expression systems, confirming the feasibility of such an approach (15, 31), we explored whether a similar strategy can be used for IL-24. Deglycosylated cytokines were reported to retain their native structures and also, whenever tested, the ability to bind cognate receptors (18). Potential advantages of bacterial expression include elimination of glycosylation that may interfere with crystallization, short expression time, and low cost. Several earlier reports addressed the problem of expressing IL-24 in bacteria (10, 11), as well as the influence of posttranslational modifications on the activity of this cytokine (7, 9). In most of these reports, however, the evidence of successful production of IL-24 in *E. coli* was limited to characterization by SDS-PAGE and mass spectroscopy (10, 11), thus preventing reliable assessment of the practicality of such approaches. Fuson et al. (7) reported *E. coli* expression of IL-24, but only in an insoluble form. The protein could be refolded in the presence of decyl-maltoside yet precipitated quantitatively after removal of the detergent. These authors also found that the yield of expression of soluble GST–IL-24 fusion was very low, and IL-24 quantitatively precipitated after the cleavage

of the GST-tag. They concluded that the solubility/stability, secretion levels, and (presumably) receptor-mediated ability to kill melanoma cells by IL-24 depend on proper *N*-glycosylation and on the presence of an intact single disulfide bond (7).

The results of our expression trials of IL-24 in *E. coli* largely mirror the earlier observations (7), particularly regarding the solubility of this cytokine, as well as the outcome of experiments involving fusion variants and refolding in the presence of detergents (data not shown). When it became clear that a refolding step is inevitable, we focused on preparation of samples devoid of any nonnative additions (i.e., affinity tags, cleavage sites, etc.) which could unfavorably affect the structure of refolded IL-24. Insoluble recombinant IL-24 could be expressed at moderate-to-high levels (20–35 mg/l), as illustrated in Fig. 1A. It should be noted that recombinant IL-24 migrates somewhat anomalously on polyacrylamide gel (SDS-PAGE), where its molecular mass appears 3–4 kDa smaller than expected. Subsequent Western blotting analysis confirmed the identity of insoluble recombinant IL-24 (Fig. 1B). IBs were extracted and washed as described in *Materials and Methods*. The wash step was followed by thorough purification using reverse-phase HPLC, resulting in highly pure, desalted polypeptide with the sequence corresponding to native mature IL-24 (aa 52–206), with an extra N-terminal methionine (an artifact of cloning and expression in bacterial cells).

Of all the tested refolding conditions, the most promising results were obtained when the initial sample of IL-24 was solubilized in 6 M guanidinium chloride, 50 mM Tris buffer (pH 7.5), at the concentration of ~1 mg/ml. The resulting solution was then diluted 50-fold by a dropwise addition to the solution containing Tris buffer, NaCl, a glutathione shuttle, Arg-HCl, and glycerol (see *Materials and Methods* for details). Dilution was associated with only minor turbidity which did not increase significantly over 24–48 h of stirring at 5°C. The solubility of such refolded IL-24 was, however, highly correlated with the presence of Arg-HCl, an antiaggregation agent, present at a concentration of 0.5 M. Removal of Arg-HCl by dialysis led to significant precipitation of IL-24, although small amounts of the cytokine remained in solution. The IL-24-containing solution was concentrated using a stirred pressure cell and subjected to size-exclusion chromatography purification. The size-exclusion chromatography elution profile indicated partial aggregation of IL-24 on the column. Fractions corresponding to nonaggregated cytokine identified by SDS-PAGE were combined and concentrated to ~3 mg/ml using a stirred pressure cell equipped with 3 kDa membrane. The protein precipitated upon any further concentration. Subsequent characterization by SDS-PAGE and mass spectrometry (see *Materials and Methods*) suggested formation of an unstable single disulfide bond in a molecule of refolded IL-24 (see Fig. 1C). The PAGE analysis of refolded IL-24, conducted under native conditions, revealed the presence of several discrete oligomeric forms (Fig. 1D). This observation, together with the results of the SDS-PAGE analysis, suggests that unstable monomers could coexist with oligomeric forms of refolded IL-24, which are stabilized by spuriously formed intermolecular disulfide bonds.

Whereas this procedure appeared to be more successful than the one previously described by Fuson and coworkers (7), as well as better than our own alternative refolding protocols, the resulting protein solution became turbid within minutes, and slowly but continuously, the bulk of IL-24 precipitated. This disappointing observation led to several conclusions. Similarly to the previous studies of refolded, deglycosylated IL-24, the cytokine aggregates in even modestly concentrated solutions, suggesting a potential role of *N*-glycosylation in its stability and solubility. The lack of a network of disulfide bonds, typically found in related cytokines,

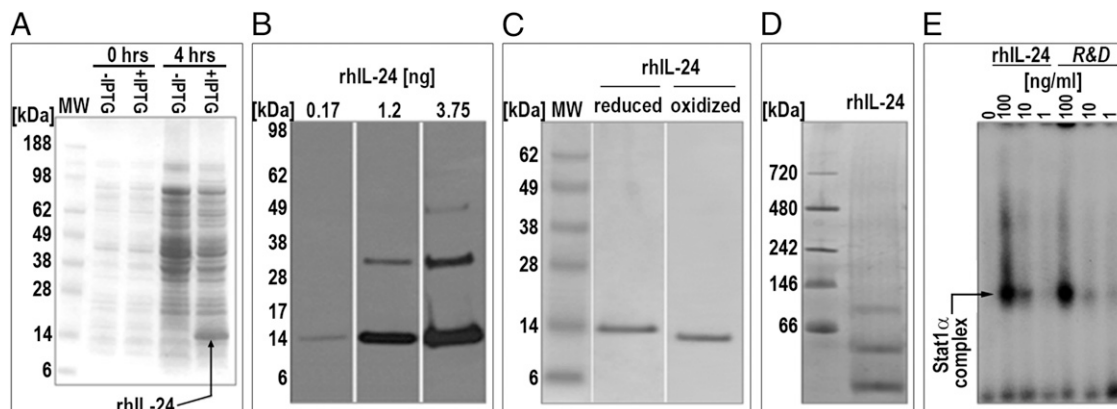


FIGURE 1. Preparation of IL-24 (*E. coli*) and its ternary complex (*Drosophila* S2). (A–E) refer to the IL-24 preparation in *E. coli*. (A) SDS-PAGE analysis of the expression of IL-24 in the BL21(DE3) pLysS cells. Lanes 2 and 3 (0 h) represent samples from the total cell lysate taken prior (–IPTG) and just after (+IPTG) induction of expression. Lanes 4 and 5 (4 h) represent samples from the total cell lysate, taken 4 h later. (B) Western blot analysis of purified insoluble IL-24 using anti-IL-24 (R&B Systems). Three samples containing different amounts of total protein are shown. Note multiple bands associated with oligomers of IL-24. (C) SDS-PAGE analysis of refolded IL-24 applied in the presence (reduced) or absence (oxidized) of 10 mM DTT. The presence of only a single band in each lane is an artifact of the small size of the sample. When larger samples were applied under the same conditions, multiple bands originating from oligomers of IL-24 were visible. (D) Electrophoresis of refolded IL-24 preparation performed under native conditions. Multiple bands corresponding to oligomers of IL-24 are seen. The two lowest bands most likely correspond to the monomer and dimer of IL-24. (E) Hamster cells expressing modified human IL-24R complex were left untreated or treated with various concentrations of recombinant *E. coli*-produced human IL-24 or mouse myeloma cell line, NS0-derived IL-24 obtained from R&D Systems (cat. no. 1965-IL; 100 ng, 10 ng, or 1 ng/ml), and STAT1 activation was tested by EMSA. Positions of STAT1 homodimers are indicated by the arrow.

may also be an important contributor to low stability. In contrast to other IL-20SFCs stabilized by three disulfide bonds each, or IL-22 by two, a molecule of IL-24 contains only two cysteines and can potentially form only a single disulfide bond (Fig. 2A). However, after incubating the solution of IL-24 at 5°C for up to 5 d, the amount of the cytokine remained in solution was sufficient for completion of the JAK-STAT signaling assay. For this purpose, we used an approach developed earlier by one of us (S.V. Kotenko), briefly outlined below.

Cytokines demonstrate various degrees of species specificity. For instance, hamster cells are not responsive to human cytokines; therefore, appropriate human receptors must be expressed in these cells to render them responsive. Such modified cells allow for easier monitoring of signaling by cytokines, which is a weak event in intact cells owing to the low level of receptor expression. In the case of IL-10–related cytokines, one receptor subunit in a receptor complex determines the specificity of signaling and subsequent biological activities (32). By substituting the intracellular domain of the signaling receptor subunit with the corresponding region of IFN- γ R1, it is possible to create new, chimeric receptors which retain their ligand-binding specificities yet gain the ability to trigger, in response to cytokine treatment, IFN- γ -specific biological activities that can be uniformly measured. Following this approach, reporter hamster cell lines expressing receptor complexes for IFNs, IL-10, IL-22, and IL-26 were previously generated (20, 33, 34). Using the same strategy, we created hamster cells expressing chimeric human IL-20R1/ γ R1 and an intact human IL-20R2, which specifically respond to IL-20SFCs. This reporter cell line was used to evaluate biological potency of recombinant IL-24. The assay was conducted in parallel for the refolded IL-24 described in this article and for a commercial sample of this cytokine (cat. no. 1965-IL-025; R&D Systems), the latter expressed in mouse myeloma cells. As can be seen in Fig. 1E, the refolded, deglycosylated IL-24 signals quite comparably to its fully glycosylated variant, indicating that in contrast to an earlier report (7), *N*-linked carbohydrates and other potential posttranslational modifications are not critical for the signaling properties of this cytokine. In conclusion, although IL-24 expressed in bacteria

binds to and activates the IL-20R1/IL-20R2 receptor complex, in its deglycosylated form this cytokine is quite unstable and prone to aggregation and is thus unsuitable for crystallographic studies.

A novel approach to preparation of ternary complexes of cytokines for structural studies

All cytokines from the IL-10 family signal by forming complexes with heterodimeric receptors. Usually, the affinity of a cytokine to one of the receptor chains is significantly lower than to the other one, at least for the soluble receptor domains (35). For example, the common IL-10R2 receptor chain, recognized by IL-10, IL-22, IL-26, and IFNs- λ , has very low affinity to cytokine ligands and is capable of binding to them only in the presence of the specific RH chain. The soluble ternary complexes of these cytokines are quite unstable, leading to difficulties in their isolation, crystallization, and structural characterization. Recently, Mendoza et al. (36) described a path to circumvent such a problem in the case of a receptor complex of IFN- λ 3. Their approach involved extensive mutagenesis of the cytokine and was labor-intensive and time-consuming. Additionally, the resulting complex contained mutations in the ligand–receptor interfaces that require *in silico* extrapolation to reconstruct the interactions present in the native complex. In this report, we present a simpler approach, in which a cytokine is tethered with the aid of a long and flexible polypeptide linker to the low-affinity receptor (RL).

Employing receptor–ligand fusions in structural studies is not a novel idea, and, for example, we previously successfully used a similar approach while studying the structure of a complex between the phage protein g3p and its bacterial coreceptor, TolA (37). In complexes of cytokines with heterodimeric receptors (RH and RL), the cytokine–receptor fusion can be generally constructed in four ways, namely cytokine-RL, RL-cytokine, cytokine-RH, and RH-cytokine. In principle, stable association of a cytokine with RH does not require covalent tethering, as shown by the available structures of several cytokine-RH binary complexes. In the case of IL-24, however, an additional complication arises from the paucity of data on its affinity for the individual receptor chains. As mentioned earlier, the failure to prepare sufficient amounts of stable IL-24

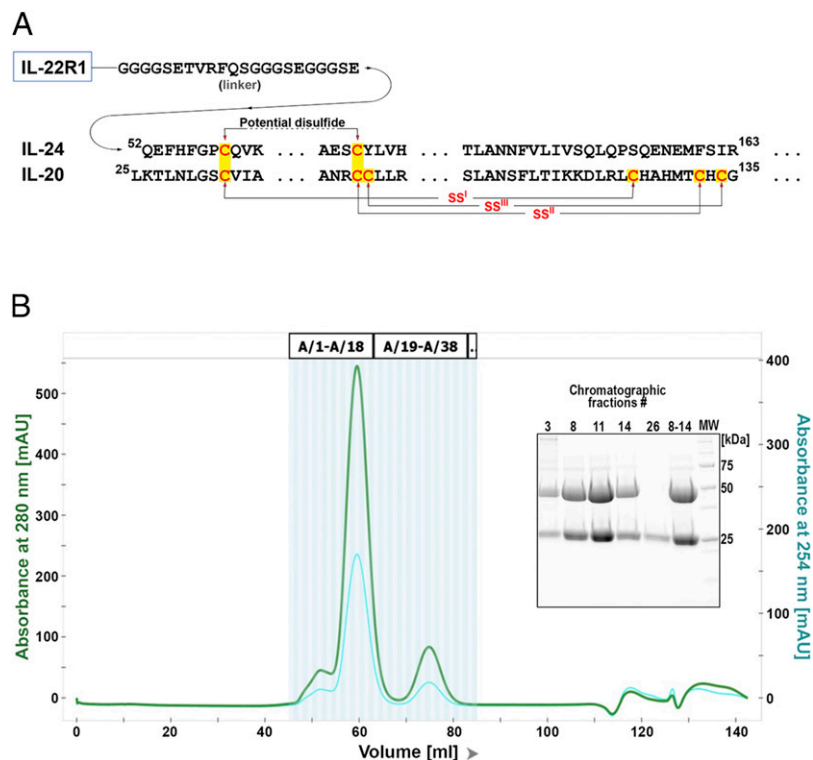


FIGURE 2. Design and expression of the IL-22R1/IL-24 fusion construct used in this study. **(A)** Schematic representation of the IL-22R1–IL-24 fusion, with fragments of IL-24 aligned with the equivalent regions of its closest homolog, IL-20. In both cytokines, the amino acid sequences are shown only for the regions containing cysteine residues, the latter shown in red font and on yellow background. The first and the last residue in each of the two cytokine sequences are numbered. Six cysteine residues present in the mature IL-20 create three disulfide bonds with indicated topology. In contrast, two cysteines present in mature IL-24 do not seem to form a stable disulfide bond (see *Results*). Additionally, the complete primary structure of the linker that fuses IL-22R1 and IL-24 is shown. **(B)** Elution profile for the ternary complex, IL-24/IL-22R1/IL-20R2, expressed in *Drosophila* S2 cells. This trace represents the final purification step on the Superdex 75 Increase column. In a subpanel (upper right side), SDS-PAGE analysis is shown for selected individual fractions collected during this purification. The fifth lane (fraction 26), corresponds to the late-eluting, minor peak, which contains an excess of the coexpressed receptor, IL-20R2. The sixth lane represents the combined fractions 8–14 containing the ternary complex, represented by bands of IL-22R1/IL-24 fusion (migrating near the 50 kDa molecular mass marker) and IL-20R2 (migrating near the 25 kDa marker). These fractions were used, after concentration, in crystallization experiments.

prevented us from quantitatively assessing affinities to individual receptor chains; thus, we could not be certain which receptor represents RL or RH. Consequently, for each of the two complexes, type I and type II, at least two fusions needed to be prepared (four, if the order of components in a fusion is considered) (i.e., IL-20R2–IL-24 and IL-20R1–IL-24 in the case of type I complex). Furthermore, it is worth noting that covalent tethering of a cytokine to its RL does not assure formation of a cytokine–RL binary complex, and only after addition of an RH chain might the advantages of the cytokine–RL fusion be realized. A long and unstructured linker, tethering noninteracting cytokine and RL molecules, may be subject to proteolytic degradation, resulting in a significantly reduced yield. The latter possibility, however, may be circumvented by the coexpression of the cytokine–RL fusion with an appropriate RH. All these scenarios were considered in our experiments conducted for the IL-24 system. A schematic diagram of the fusion construct successfully used for structural studies is shown in Fig. 2A.

When IL-24 was expressed in the absence of a receptor or fused to IL-20R2 (in both cytokine–receptor and receptor–cytokine configurations), the yields of expression in insect cells were very low (albeit detectable by Western analysis). Some increase in the yield was observed for expression of IL-20R1–IL-24 or IL-22R1–IL-24 fusions; however, when the latter fusion was coexpressed with IL-20R2, the yield increased dramatically (see Fig. 2B), reaching tens of milligrams per liter of *Drosophila* cell culture. The ternary complex formed during this experiment could be readily

purified and its identity was confirmed by SDS-PAGE and Western analysis.

Crystal structure of the IL-24/IL-22R1/IL-20R2 complex

Crystal structure of the complex of IL-24 with two receptors, IL-22R1 and IL-20R2, was determined by molecular replacement using data extending to the resolution of 2.15 Å. Diffraction data were collected from one tetragonal crystal in space group $P4_3$, with a single complex in the asymmetric unit (Table I). The structure was solved by molecular replacement with the program PHASER (24) with the coordinates of the IL-20/IL-20R1/IL-20R2 ternary complex [PDB ID: 4doh (13)] used as the search model. The initial solution was optimized with MR Rosetta (26), and the structure was rebuilt with Coot (28) and refined with Refmac5 (27) to R_{work} of 0.183 and R_{free} 0.225 (Table II). Unlike what was reported in the case of the complex of IL-20/IL-20R1/IL-20R2, for which a dimer was present in the asymmetric unit (13), a limited number of crystal contacts seen in the structure of the IL-24 complex does not suggest any oligomerization. Even though molecules of IL-24 and IL-22R1 were fused into a single chain, the linker residues were completely disordered; thus, in the following description these two proteins are numbered as two independent chains. Whereas a majority of quality indicators of this structure are in an acceptable range, three indicators (i.e., the individual B-factors, Z-score of the real space R value), and the overall small number of water molecules may appear unsatisfactory when compared with structures of many

Table I. Statistics for diffraction data collection and processing

Diffraction source	Beamline 22-ID, SER-CAT, APS, ANL
Wavelength (Å)	1.0000
Temperature (K)	100
Detector	Rayonix 300-HS high speed CCD
Crystal-to-detector distance (mm)	270
Rotation range per image (°)	1.0
Total rotation range (°)	360
Exposure time per image (s)	1.0
Space group	$P4_3$
<i>a</i> , <i>b</i> , <i>c</i> (Å)	77.70, 77.70, 124.79
Mosaicity (°)	0.25–0.90
Resolution range (Å)	99.00–2.15 (2.23–2.15) ^a
Total no. of reflections	317,252
No. of unique reflections	39,903
Completeness (%)	99.7 (100)
Multiplicity	8.0 (7.1)
$\langle I/\sigma(I) \rangle$	29.7 (1.62)
R_{merge}^b	0.072 (1.416)
R_{pim}^c	0.034 (0.62)
$CC_{1/2}^d$	0.97 (0.70)

^aValues in parentheses are for the highest-resolution shell.

^b $R_{\text{merge}} = \sum_{hkl} (|I_{hkl} - \langle I_{hkl} \rangle|) / \sum_{hkl} I_{hkl}$.

^c $R_{\text{pim}} = \sum_{hkl} \sqrt{(1/n-1) \sum_j |I_{hkl,j} - \langle I_{hkl} \rangle|} / \sum_{hkl} \sum_j I_{hkl,j}$, where *n* is the multiplicity of data.

^d $CC_{1/2}$, Pearson correlation coefficient between two randomly selected halves of the data set.

ANL, Argonne National Laboratory; APS, Advanced Photon Source; SER-CAT, Southeast Regional Collaborative Access Team.

globular proteins determined at a similar resolution. However, this phenomenon is common for ternary complexes of cytokines and was similarly manifested, for example, in the structures of the IL-20–IL-20R1–IL-20R2 complex [PDB ID: 4doh (13)] and IFN- λ 3–IFN- λ R1–IL-10R2 complex [PDB ID: 5t5w (36)]. Such behavior is due to the dynamic nature of the whole complexes and, particularly, to plasticity of the receptor molecules.

Structure of IL-24 and its comparison with the structures of related cytokines

The IL-24 gene encodes 206 aa, of which the first 51 represent the signal sequence. The construct used in this study starts with Q52 and ends with L206 (the numbering used throughout accounts for the residues belonging to the signal peptide), with all amino acids in between modeled in the electron density without any breaks, in contrast to some previously reported structures of related cytokines. As is also the case of IL-20, the structure of which was only determined in a complex with its receptors, no structural data are available for IL-24 alone, making the structure described in this article the first one for this cytokine, to our knowledge. The fold of IL-24, which it shares with other helical cytokines, is called a four-helix-bundle, despite actually containing six helices (Fig. 3A, 3F). The N-terminal residues Q52–K62 form a β hairpin, similar to the one previously seen in IL-20 (Fig. 3A, 3F). The α 1 helix extends from P66 through D84 and is followed by an irregular chain and a very short helix α 2 (Q94–Q98). Helix α 3 extends from E104 through Q126, whereas R132–Q150 form helix α 4. The helix α 5 (S161–L180) is connected by a short linker to helix α 6 (E183–F203). Although C59 is located in close vicinity of C106, both poised to form a disulfide bridge, the electron density does not support its existence. Whereas the side chain of C59 appears to be well ordered, the side chain of C106 accommodates two different conformations (Fig. 4). When the SG atom of the latter residue points at SG of C59, the closest distance of their approach is 2.74 Å (Fig. 4A), which is significantly longer than the typical disulfide bond distance of 2.05 Å. The attempts to force

Table II. Refinement statistics

Resolution range (Å)	30.0–2.15 (2.21–2.15) ^a
Completeness (%)	99.7 (98.9)
σ cutoff	None
No. of reflections, working set	37,892 (2730)
No. of reflections, test set	1978 (165)
Final R_{work}	0.183 (0.297)
Final R_{free}	0.225 (0.318)
No. of non-H atoms	
Protein	4395
Water	80
Carbohydrate	42
Other heterogens	12
Total	4529
Root mean square deviations	
Bonds (Å)	0.019
Angles (°)	1.957
Average B-factors (Å ²)	
Protein	76.5
Water	62.5
Total	74.7
Ramachandran plot ^b	
Favored regions (%)	96.6
Additionally allowed (%)	2.8
Disallowed regions (%)	0.6 (G61, G175, G198) ^c
No. of complexes in asymmetric unit	1
PDB code	6DF3

^aOutermost shell.

^bStatistics were calculated with the Web-based version of MolProbity [http://molprobity.biochem.duke.edu/ (29)].

^cAll three glycines are in the loop regions of IL-20R2.

the presence of this disulfide during refinement did not succeed and the electron density quite clearly supported the interpretation presented here (Fig. 4B–D). Therefore, one can conclude that this disulfide is formed under some conditions (as shown by mass spectrometry of the refolded IL-24 expressed in *E. coli*), although it is not seen in the current structure.

Superposition of the coordinates of molecule A of IL-20 from the ternary complex of that cytokine (PDB ID: 4doh) onto IL-24 yields a root mean square deviation 1.3 Å for 123 pairs of C α atoms. Such a close similarity is present despite only limited amino acid sequence identity of these cytokines (29%). Both cytokines contain an N-terminal β hairpin, although insertion of G63 in IL-24 (absent in IL-20) leads to its significant distortion. Relative placement of helix α 2 and the conformation of the following residues (Q98–Q99) differ because no corresponding motif is present in IL-20 (Fig. 3E). Helix α 3 is longer in IL-24 than in IL-20, leading to significant structural differences for residues H125–R127 (Fig. 3B). Positions of the C α atoms in the loop connecting helices α 4 and α 5 (P153–I162) differ by as much as 8.5 Å owing to the presence of an additional turn in the helix α 4 of IL-20. Finally, IL-24 contains two additional residues on its C terminus (K205 and L206).

Sequence identity between IL-24 and IL-19 is 28.5% (similar to the identity with IL-20), and the RMSD is 1.4 Å between 133 equivalent C α atoms of the two cytokines. Nevertheless, structures of the amino termini of both of them differ significantly, most certainly because of the presence of an additional α helix in IL-19 (PDB ID: 1n1f), replacing the β hairpin in IL-24. Other areas of differences include helix α 2, the C terminus of helix α 3, and the connector chain between helices α 4 and α 5 (the latter being virtually identical in IL-19 and IL-20). The C terminus is shorter in IL-24 than in IL-19 and points in a different direction.

IL-22 differs more from IL-24 than from the other two closely related cytokines, with the sequence identity of only 19.8%. When the chain I (IL-22) in the complex of IL-22 with IL-22R1 (PDB ID: 3dlq; this entry represents one of the two available structures of

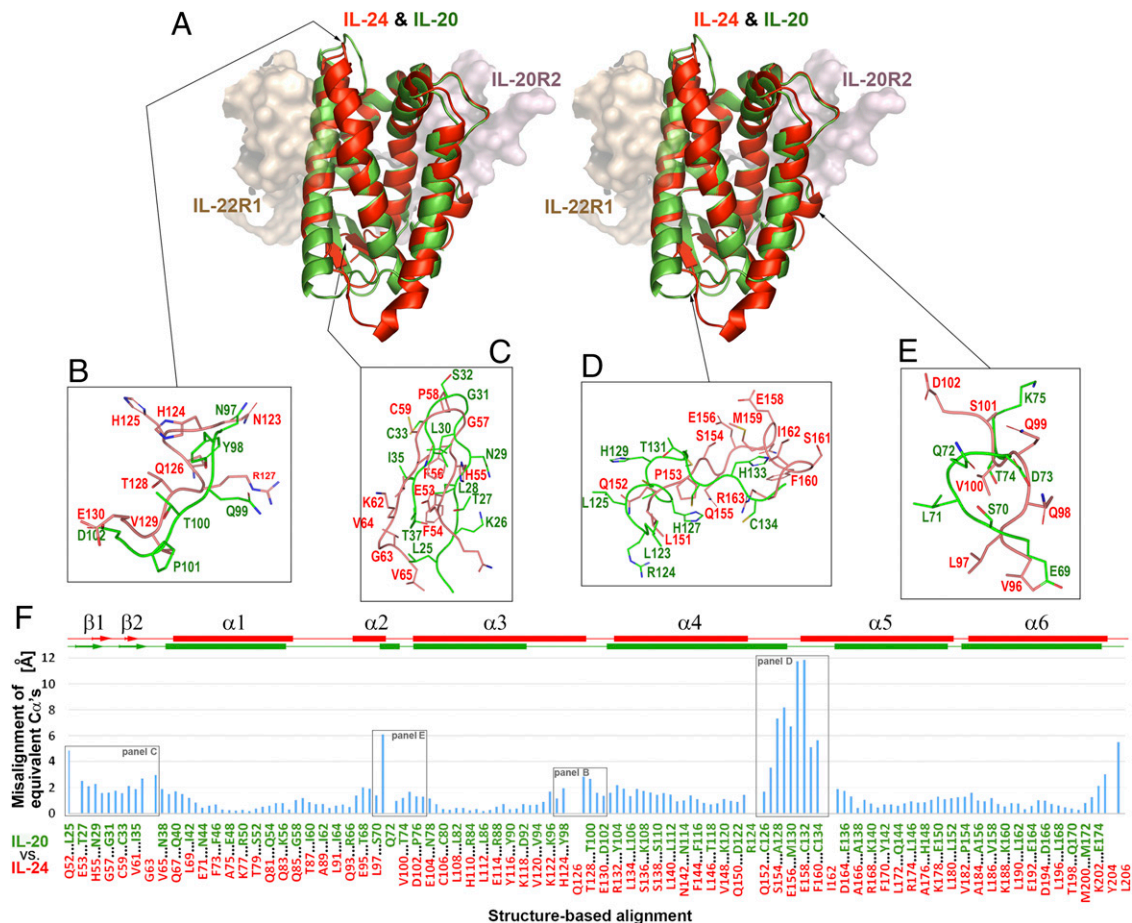


FIGURE 3. Topology of IL-24 compared with its closest homolog, IL-20. **(A)** A cartoon of the superimposed IL-24 (red) and IL-20 (green). The cytokines are flanked by fragments of the two receptors (shown as semitransparent surfaces), oriented as in the IL-24/IL-22R1/IL-20R2 ternary complex. As expected, the overall topologies of IL-24 and IL-20 are very similar. However, due to differences in the chain lengths and amino acid sequences, several equivalent regions are structurally divergent. These fragments are almost exclusively located at the apices of the four-helix-bundle cores of both cytokines. **(B–E)** Four examples of regions diverging between IL-24 and IL-20. In each case, main-chain atoms are represented as ribbons and side chains as sticks. Most of the depicted amino acid residues are labeled. The approximate locations of these four regions within the superimposed IL-24 and IL-20 molecules are indicated by arrows. **(F)** Distances between the equivalent C α atoms from the two structurally aligned cytokines illustrated as a bar graph. For clarity, every other pair of equivalent residues is annotated on the horizontal axis. Locations of structurally divergent regions of IL-24 and IL-20, highlighted in **(B–E)**, are indicated by black frames. Secondary structure elements in both cytokines are shown above the bar graph.

IL-22/IL-22R1, which is refined at higher resolution) is compared with IL-24, the RMSD is 2.23 Å for 121 equivalent C α atoms. The linking region between helices α 4 and α 5 is not observed in that structure of IL-22. This region, however, is ordered in the structure of uncomplexed IL-22 (PDB ID: 1m4r), but the difference in chain length between IL-22 and IL-24 leads to deviations in positions of equivalent C α atoms exceeding 6 Å.

Structures of the receptors in the complex with IL-24

Structures of both IL-22R1 and IL-20R2 have been determined in the past (13, 17, 18). Two copies of IL-22R1 are present in one of the structures of its binary complex with IL-22 (PDB ID: 3dgc), the components of which were expressed in insect cells. One of the molecules of the receptor is clearly glycosylated at N172, whereas no presence of the carbohydrate moiety can be detected in the other molecule. Only one molecule of IL-22R1 is present in the other similar complex (PDB ID: 3dlq), with both proteins expressed in *E. coli* and thus not glycosylated. In the structure described in this article (Fig. 5A, 5B), IL-22R1 is clearly *N*-glycosylated at N80 and N87, although no modification of the N172 side chain was found. Both previously determined structures indicated the presence of a disulfide formed between C71 and C79, whereas no

such bond is seen in the current structure. Although the thiol groups from both cysteines point toward each other, in the refined structure, distance between S γ atoms (3.1 Å) significantly exceeds the length of a standard disulfide bond (2.05 Å), and a negative electron density peak is present between these atoms. We interpret this result as showing that this disulfide might be labile. Such interpretation is additionally supported by the presence of significant negative electron density in the middle of the corresponding disulfide in 3dlq and in one of such disulfides in 3dgc, suggesting that their supposed presence may have been forced by the refinement procedures. Superposition of IL-22R1 in the complex discussed in this article onto the receptor (chain R in the PDB entry 3dgc) yields RMSD of 0.74 Å for 193 C α pairs, whereas RMSD is 0.77 Å in a superposition with the equivalent receptor molecule in the PDB entry 3dlq. By comparison, superposition of the two receptor molecules in 3dgc yields RMSD of 0.89 Å for 202 equivalent C α pairs. Despite the differences in expression protocols for both samples and nonidentical crystal contacts, the models of IL-22R1 are remarkably similar.

The only previously published structure of IL-20R2 is in a ternary complex of IL-20 [PDB ID: 4doh (13)]. The receptor was expressed in insect cells, but the potential *N*-glycosylation sites were removed by mutating N40 and N134 to Glu. Although only

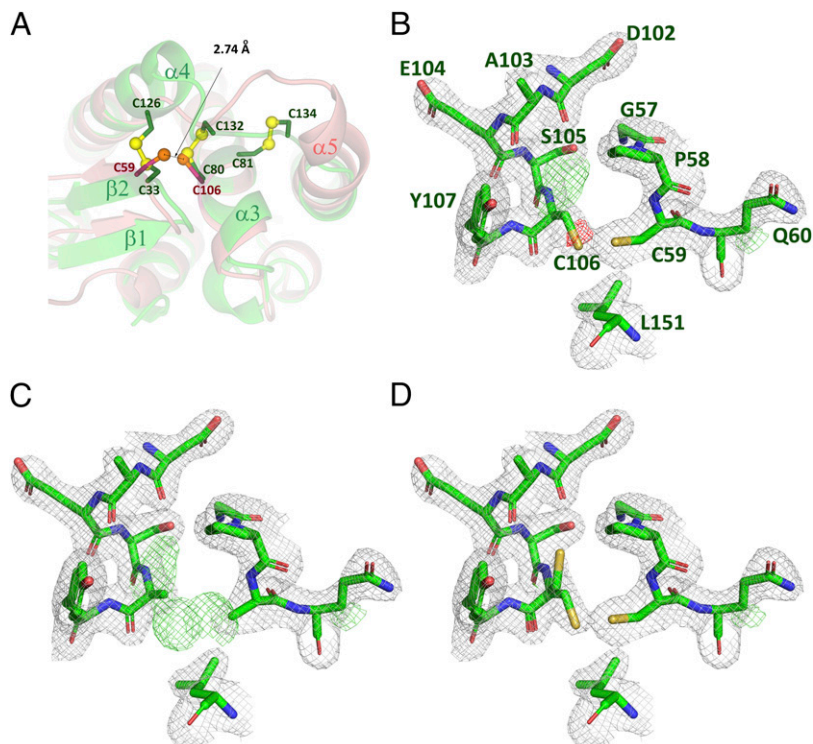


FIGURE 4. Cysteine residues in human IL-24. **(A)** An apex of the bottom of the four-helix-bundle of IL-24 (pale red) and IL-20 (pale green) superimposed as in Fig. 1. Visible secondary structure elements and cysteine residues are labeled. In contrast to six cysteines forming three disulfide bonds in IL-20, only two Cys residues, C59 and C106, are present in IL-24. The closest distance between S γ atoms in the refined structure is 2.74 Å, indicating the absence of a covalent Cys–Cys linkage. This interpretation is supported by the electron density calculated with different refined models. **(B)** When both Cys residues were modeled and refined with single conformations, negative density on S γ of C106 and strong positive density next to it indicates the presence of a second conformation. **(C)** When both cysteines are refined as Ala, the electron density map indicates a single orientation of C59 and two orientations of C106. **(D)** The best agreement between the model and electron density is achieved when C106 is modeled in two alternate conformations. However, neither conformer positions the S γ atom of C106 sufficiently close (<2.1 Å) to the S γ atom of C59 to postulate formation of a stable covalent bond, and enforcement of the disulfide formation through external restraints was not compatible with the experimental diffraction data. In **(B)**–**(D)**, the 2mFo–DFc electron density map (light gray) is contoured at 1.1 σ , whereas the mFo–DFc map is contoured at $\pm 3\sigma$ (green and red, respectively).

N134 was mutated in the IL-24 complex discussed in this article, there is no indication in the electron density map that N40 was *N*-glycosylated. Superposition of the two structures yields RMSD 0.94 Å for 190 equivalent C α pairs, with the only significant differences (~ 3 Å) in the loop around P60.

Interactions between IL-24 and its receptors

Interactions between IL-24 and its receptors, as well as between IL-22R1 and IL-20R2, were evaluated with the program *Contact* in CCP4 (38), as well as with servers PDBePisa (<http://www.ebi.ac.uk/pdbe/pisa/>) and CCharPPI (<https://life.bsc.es/pid/ccharppi>). Computational estimation of the binding energy for a protein–protein interface in a crystallographic structure or a molecular model is a notoriously challenging problem. There have been developed dozens of computational tools based on different empirical or analytic approaches; however, their performance varies based on a particular kind of protein, and it is difficult to pinpoint a single one that would universally provide a reliable quantification (39).

According to PDBePisa, the primary contribution to complex formation is provided by interactions between IL-24 and IL-20R2 (Fig. 5C). The interface area between these molecules extends over 875 Å² and involves 13 hydrogen bonds. With the exception of the carbonyl oxygen of L117 of IL-24, all other H-bonded atoms of the cytokine are contributed by amino acid side chains (Q52, Q126, K135, S138, T139, N142, N143, and Y204). Ten hydrogen bonds are made by the side chain atoms Y70, Y74, E75, H81, D102, T104, and K210 of IL-20R2; however, the main

chain peptide carbonyl oxygen of T104 and amide nitrogen atoms of E73 and Y74 are also involved. Two interactions (H125–E75 and K135–D102) represent potential salt bridges. Several additional polar contacts use well-ordered water molecules residing within interfaces (i.e., Wat13 lodged between the amide nitrogen of T106 of the receptor and the carbonyl oxygen of G63, as well as OD1 of N143 of the cytokine). Another water-mediated contact involves Y109 OH of the receptor and S138 OG of IL-24 (Wat8). Finally, a number of hydrophobic contacts stabilize the interactions between the receptor and the cytokine. Examples include the side chains of I84 of IL-20R2 and L134 of IL-24 or the extensive contacts of the ring of Y74 of the receptor with Ala41 and F121 of IL-24. The energy gain computed with PDBePISA and due to the high-affinity interaction between IL-24 and IL-20R2 is significant ($\Delta^{\dagger}G = 9.1$ kcal/mol).

Although the interface area between IL-24 and IL-22R1 (Fig. 5C) is slightly larger (961 Å²) and involves a larger number of hydrogen bonds between the cytokine and the receptor (17), the stabilization energy estimated by PDBePISA is quite modest ($\Delta^{\dagger}G = 1.7$ kcal/mol). The hydrogen bonds within this interface engage the side chains of W74, K77, D84, T87, R90, Q94, K188, E192, and D194 of IL-24 as well as the main chain carbonyl oxygens of T87, A89, G191, and Y204. The counterparts contributed by IL-22R1 are the side chains of K58, Y60, E90, R112, Q117, and H161 as well as main chain carbonyl oxygens of T89 and T207 and the amide nitrogen atom of G61. Salt bridges are made by R90–E90 and D84–R112 of IL-24 and IL-22R1, respectively. No clearly defined water molecules

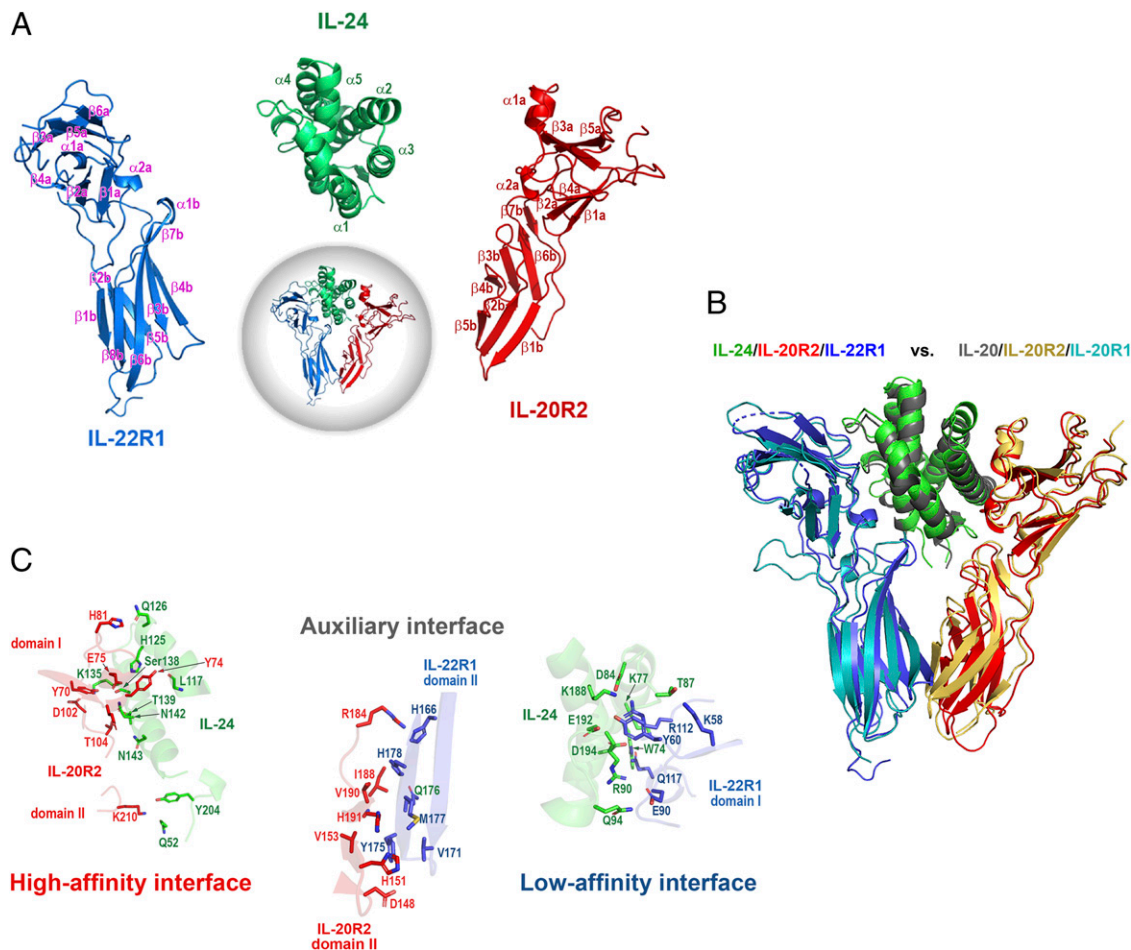


FIGURE 5. Ternary complex of human IL-24 with soluble domains of IL-22R1 and IL-20R2. **(A)** A cartoon representation illustrating the overall architecture of the complex is shown at the center, with IL-24 colored green, IL-22R1 in blue, and IL-20R2 in red. The image of the complex is flanked by enlarged depictions of three component molecules at unchanged orientations, with secondary structure elements indicated. Each of the receptor chains is formed by two fibronectin type III domains, indicated in the figure as “a” and “b” within labels annotating the secondary structure elements. The topologies of individual chains as well as of the whole complex are typical for this family of cytokines. **(B)** The ternary complex of IL-24 is superimposed on the type I complex of IL-20 [IL-20–IL-20R1–IL-20R2; PDB ID: 4doh (13)], based on structurally-equivalent C α atoms from all chains. A description of the coloring scheme is shown above the cartoon. Whereas it is quite apparent that topologies of both ternary complexes are quite similar, relative displacements of specific regions are quite clear (see the main text for more detail). **(C)** Three interfaces contributing to complex stabilization. Topological elements of molecules forming the interfaces are represented as semitransparent cartoons colored as in the other panels. Side chains of residues that contribute to stabilization of interfaces are shown as sticks, and most of them are labeled.

mediate the receptor–cytokine interactions, although Wat67, despite its high B factor, may link the carbonyl oxygen of G61 of IL-22R1 with the amide nitrogen of R90 of IL-24. The most prominent hydrophobic interaction involves W208 of the receptor and W70 of the cytokine.

The interface between the two receptor chains (Fig. 5C) is much smaller (441 Å², $\Delta^1G = 2.4$ kcal/mol), with only four hydrogen bonds involving the side chains of D148 and K181, as well as the main chain carbonyl oxygen of P189 and the amide nitrogen of H191 in IL-20R2, paired with the side chain of N172, main chain carbonyl atoms of Q176 and H178, and the amide nitrogen of Q176 of IL-22R1. The only observed water-mediated contact involves Wat58 interacting with the amide nitrogen of H178 of IL-22R1 and the carbonyl oxygen of H191 of IL-20R2.

The numerical results obtained with the CCharPPI server are somehow different from the estimates provided by PDBePISA. This server provided a “collective” estimate using 106 different scoring functions developed by different groups. We have correlated the scores with the binding energy using the benchmark dataset of the proteins with experimentally measured binding (30).

The estimates were performed separately for IL-22R1/IL-24 and IL-20R2/IL-24 interfaces. For both interfaces, the binding energies were comparable, on the scale of ~ 11 kcal/mol. Nevertheless, the majority of estimates predict the binding at IL-20R2 interface as slightly stronger, typically in the range of 0.1–0.4 kcal/mol, which is considerably smaller than the energy of a typical hydrogen bond. This analysis estimates the total binding energy for IL-24 to be around 22 kcal/mol, and it does not directly answer the question of which receptor is primary versus secondary, although it still indicates that IL-20R2 may play a role of the former one.

Discussion

In this work, we have determined the crystal structure of the type II ternary complex between human IL-24 and the extracellular domains of two receptors, IL-22R1 and IL-20R2. This is only a third example of a ternary complex for a cytokine from the IL-10 family and, to our knowledge, the first detailed structural characterization of IL-24. IL-24 is more difficult to prepare in a stable form than most cytokines from the IL-10 family. Its main difference from the other members of this family, in particular other IL-20SFCs, is the

low content of Cys residues. Whereas most of the related cytokines are stabilized by two or three intramolecular disulfide bonds, the two cysteines in IL-24 can only form a single intramolecular disulfide, which appears to be unstable. It was previously suggested that *N*-glycosylation and the formation of a single disulfide bond are both needed for manifestation of biological activities of IL-24 (7). The results of our attempts to prepare stable and functional IL-24 from bacterial cultures were only partially consistent with those earlier observations. Although preparations of deglycosylated IL-24 were quite unstable, sufficient remaining quantities of the properly folded, soluble cytokine could still engage productively with cognate receptors and initiate the JAK/STAT signaling pathway at concentrations comparable to fully *N*-glycosylated commercial sample of IL-24, which originated from mammalian source. These data showed that similarly to many other cytokines, *N*-glycosylation of IL-24 is dispensable for receptor signaling. In contrast, whether fully deglycosylated IL-24 displays the same range of structural features and biological activities as its natural variant still remains unclear. For example, full glycosylation may enforce and stabilize a disulfide bond between two Cys residues of IL-24, the bond which was not unambiguously detected in present studies. Our initial results obtained with refolded preparations of IL-24 suggested that the presence of carbohydrate may determine the stability (reflected by solubility and tendency for aggregation) of this cytokine. However, crystal structure of the IL-24 complex suggests an additional possibility. We found that the two Cys residues do not contribute much to stabilization of the cytokine through formation of a disulfide bond, which, if formed, is likely labile or transient. In turn, the tendency of IL-24 to aggregate is eliminated in the complex by stabilization provided by the receptor chains. In contrast, inclusion of receptors practically eliminates an ability to discriminate between contributions of *N*-glycosylation and/or the disulfide bond to the structural stabilization of IL-24.

The destabilization of IL-24 by the apparent lack of a disulfide bridge between two Cys residues may provide a molecular mechanism ensuring localized and temporary action of IL-24. For example, it was reported that expression of IL-24 in rats was transiently elevated at the skin wound edges and base with the gradual decline of its expression during wound healing process (40). Thus, the following scenario is feasible when IL-24 produced after skin injury would act only in the vicinity of the wound, because only keratinocytes expressing the IL-24R would bind and respond to this locally produced cytokine. Excess of the unbound IL-24 would be quickly degraded because of its low stability without receptor binding. Other IL-10-related cytokines that act through the same receptor but are more stable than IL-24 may provide a long-range action and similar biological activities, and the differential functions of IL-24 and other cytokines may be achieved through their distinct expression kinetics and cellular sources.

The inability to prepare sufficient quantities of pure IL-24 in free form prevented us from directly determining the receptor-binding properties of this cytokine. Although it was demonstrated before (41) and was also shown in this study that IL-24 induces receptor signaling at low nanomolar concentrations, these results originate from experiments in which intact transmembrane receptor chains are present. The results reported in this study provide, at best, an indirect evidence that the shared receptor, IL-20R2, binds to IL-24 with slightly higher affinity than either IL-20R1 or IL-22R1. Whereas our conclusion is indirect, when combined with the previously published data for IL-19 and IL-20 (13, 35), it indicates that IL-20R2 may play the role of the RH of IL-20SFCs. This observation is contrary to the other subgroup of the IL-10 family members, those

utilizing the IL-10R2 receptor chain, in which this shared receptor is invariably the low-affinity component.

The overall topology of the IL-24 ternary complex described in this study is very similar to the one described earlier for IL-20 (Fig. 5A, 5B) (13). Local structural differences between both complexes are partly attributed to low amino acid sequence identity between IL-24 and IL-20 and, more importantly, to the differences in the disulfide networks. These structural differences seem too subtle to explain the differences between the biological properties of IL-24 and other IL-20SFCs, particularly IL-20, which shares identical receptor complexes. Most likely, differences in biological responses to these cytokines result from specific patterns of their expression, their different tissue and cellular distribution, and activation profiles, and are less related to their structures. However, it is tempting to speculate that unique physicochemical properties of IL-24 may play a role in its activities that are not dependent on interactions with its receptors. In contrast to other IL-20SFCs, antitumor properties of IL-24 were recognized early on, but the specific molecular mechanisms behind a direct involvement or as an adjuvant are poorly understood.

A major breakthrough in our efforts to determine the structure described in this report was introduction of the strategy utilizing receptor–ligand fusions. The use of multicomponent fusions in structural studies is not new; however, we are not aware of any earlier reports describing such a strategy for structural studies of cytokine complexes. The original motivation for utilizing this approach was to stabilize IL-24. That goal, in principle, could be achieved by linking IL-24 to its RH, if such a fusion could be expressed in quantities needed for structural studies. In our study, this proved to not be the case. Because we had no prior knowledge about the affinity of IL-24 toward individual receptor chains, many plasmids encoding different IL-24 fusions were prepared and tested for expression. During this process, we realized that additional factors that were not IL-24 specific could be incorporated in the protocol, of which the most significant was the concept of fusing the cytokine to its RL chain (in contrast to IL-24, for most of the IL-10 family members, data on receptor affinities is available). It is well known that a subgroup of IL-10-related cytokines, sharing IL-10R2, binds it with very low affinity, usually precluding formation of stable ternary complex by a simple mixing of individual components. In a somewhat fortuitous way, we found that the IL-22R1–IL-24 fusion (but not the IL-20R2–IL-24 fusion), particularly in the presence of IL-20R2, was expressed at high levels.

Based on our studies of other cytokines from the IL-10 family, we believe that the strategy outlined in this article may be generally useful in preparation of other ternary complexes (data not shown). If applicable, it accomplishes two goals: providing a stoichiometric ratio of a cytokine and its RL, and assuring mutual access of both molecules. However, a few additional considerations should be taken into account. The optimal arrangement of the components in a fusion (i.e., RL-cytokine instead of cytokine-RL) and the structure of the linker (length and composition) may require testing in each individual case. Whereas coexpression of the RL-cytokine fusion with RH was shown to be most successful for the IL-24 complex, in at least one other case we found that the RL-cytokine fusion was expressed at a very high level even in the absence of RH. In that particular case, a ternary complex was subsequently formed by mixing the purified RL-cytokine fusion with an excess of RH (data not shown). When the ternary complex is a result of coexpression, it may be necessary to supply additional amounts of RH during purification to assure stoichiometry. This would be the case when the expression level of the RL-cytokine fusion is lower than that of RH and separation of the ternary complex from an excess of the fusion might not be trivial. Inclusion of a specific

cleavage site within the linker is, in our opinion, of secondary importance. In the cases when interactions between an isolated RL and cytokine or between RL and cytokine/RH binary complex are weak, cleavage of the linker will most likely result in dissociation of the ternary complex.

Acknowledgments

Data were collected at Southeast Regional Collaborative Access Team 22-ID beamline at the Advanced Photon Source, Argonne National Laboratory. Supporting institutions may be found at www.ser-cat.org/members.html.

Disclosures

The authors have no financial conflicts of interest.

References

- Jiang, H., J. J. Lin, Z. Z. Su, N. I. Goldstein, and P. B. Fisher. 1995. Subtraction hybridization identifies a novel melanoma differentiation associated gene, mda-7, modulated during human melanoma differentiation, growth and progression. *Oncogene* 11: 2477–2486.
- Jiang, H., Z. Z. Su, J. J. Lin, N. I. Goldstein, C. S. Young, and P. B. Fisher. 1996. The melanoma differentiation associated gene mda-7 suppresses cancer cell growth. *Proc. Natl. Acad. Sci. USA* 93: 9160–9165.
- Whitaker, E. L., V. A. Filippov, and P. J. Duerksen-Hughes. 2012. Interleukin 24: mechanisms and therapeutic potential of an anti-cancer gene. *Cytokine Growth Factor Rev.* 23: 323–331.
- Menezes, M. E., S. Bhatia, P. Bhoopathi, S. K. Das, L. Emdad, S. Dasgupta, P. Dent, X. Y. Wang, D. Sarkar, and P. B. Fisher. 2014. MDA-7/IL-24: multifunctional cancer killing cytokine. *Adv. Exp. Med. Biol.* 818: 127–153.
- Persaud, L., D. De Jesus, O. Brannigan, M. Richiez-Paredes, J. Huaman, G. Alvarado, L. Riker, G. Mendez, J. Dejoie, and M. Sauane. 2016. Mechanism of action and applications of interleukin 24 in immunotherapy. *Int. J. Mol. Sci.* 17: E869.
- Zdanov, A. 2004. Structural features of the interleukin-10 family of cytokines. *Curr. Pharm. Des.* 10: 3873–3884.
- Fuson, K. L., M. Zheng, M. Craxton, A. Pataer, R. Ramesh, S. Chada, and R. B. Sutton. 2009. Structural mapping of post-translational modifications in human interleukin-24: role of N-linked glycosylation and disulfide bonds in secretion and activity. *J. Biol. Chem.* 284: 30526–30533.
- Gupta, P., Z. Z. Su, I. V. Lebedeva, D. Sarkar, M. Sauane, L. Emdad, M. A. Bachelor, S. Grant, D. T. Curiel, P. Dent, and P. B. Fisher. 2006. mda-7/IL-24: multifunctional cancer-specific apoptosis-inducing cytokine. *Pharmacol. Ther.* 111: 596–628.
- Sauane, M., P. Gupta, I. V. Lebedeva, Z. Z. Su, D. Sarkar, A. Randolph, K. Valerie, R. V. Gopalkrishnan, and P. B. Fisher. 2006. N-glycosylation of MDA-7/IL-24 is dispensable for tumor cell-specific apoptosis and “bystander” antitumor activity. *Cancer Res.* 66: 11869–11877.
- Liu, J. J., B. F. Zhang, X. X. Yin, D. S. Pei, Z. X. Yang, J. H. Di, F. F. Chen, H. Z. Li, W. Xu, Y. P. Wu, and J. N. Zheng. 2012. Expression, purification, and characterization of RGD-mda-7, a His-tagged mda-7/IL-24 mutant protein. *J. Immunoassay Immunochem.* 33: 352–368.
- Amirzada, M. I., M. Yu, X. Gong, Y. Chen, R. Zhu, J. Lei, and J. Jin. 2014. Cost-effective production of recombinant human interleukin 24 by lactose induction and a two-step denaturing and one-step refolding method. *J. Ind. Microbiol. Biotechnol.* 41: 135–142.
- Dumoutier, L., C. Leemans, D. Lejeune, S. V. Kotenko, and J. C. Renaud. 2001. Cutting edge: STAT activation by IL-19, IL-20 and mda-7 through IL-20 receptor complexes of two types. *J. Immunol.* 167: 3545–3549.
- Logsdon, N. J., A. Deshpande, B. D. Harris, K. R. Rajashankar, and M. R. Walter. 2012. Structural basis for receptor sharing and activation by interleukin-20 receptor-2 (IL-20R2) binding cytokines. *Proc. Natl. Acad. Sci. USA* 109: 12704–12709.
- Chang, C., E. Magracheva, S. Kozlov, S. Fong, G. Tobin, S. Kotenko, A. Wlodawer, and A. Zdanov. 2003. Crystal structure of interleukin-19 defines a new subfamily of helical cytokines. *J. Biol. Chem.* 278: 3308–3313.
- Nagem, R. A. P., D. Colau, L. Dumoutier, J.-C. Renaud, C. Ogata, and I. Polikarpov. 2002. Crystal structure of recombinant human interleukin-22. *Structure* 10: 1051–1062.
- Xu, T., N. J. Logsdon, and M. R. Walter. 2005. Structure of insect-cell-derived IL-22. *Acta Crystallogr. D Biol. Crystallogr.* 61: 942–950.
- Jones, B. C., N. J. Logsdon, and M. R. Walter. 2008. Structure of IL-22 bound to its high-affinity IL-22R1 chain. *Structure* 16: 1333–1344.
- Bleicher, L., P. R. de Moura, L. Watanabe, D. Colau, L. Dumoutier, J. C. Renaud, and I. Polikarpov. 2008. Crystal structure of the IL-22/IL-22R1 complex and its implications for the IL-22 signaling mechanism. *FEBS Lett.* 582: 2985–2992.
- Cruz, A., B. Nguyen, M. Sauane, and G. E. Lopez. 2016. Structural and functional characterization of Interleukin-24 based on atomistic molecular modeling. *Chem. Lett.* 45: 327–329.
- Kotenko, S. V., L. S. Izotova, B. P. Pollack, T. M. Mariano, R. J. Donnelly, G. Muthukumar, J. R. Cook, G. Garotta, O. Silvennoinen, J. N. Ihle, et al. 1995. Interaction between the components of the interferon gamma receptor complex. *J. Biol. Chem.* 270: 20915–20921.
- Kotenko, S. V., G. Gallagher, V. V. Baurin, A. Lewis-Antes, M. Shen, N. K. Shah, J. A. Langer, F. Sheikh, H. Dickensheets, and R. P. Donnelly. 2003. IFN-lambdas mediate antiviral protection through a distinct class II cytokine receptor complex. *Nat. Immunol.* 4: 69–77.
- Yuan, J., U. M. Wegenka, C. Lütticken, J. Buschmann, T. Decker, C. Schindler, P. C. Heinrich, and F. Horn. 1994. The signalling pathways of interleukin-6 and gamma interferon converge by the activation of different transcription factors which bind to common responsive DNA elements. *Mol. Cell. Biol.* 14: 1657–1668.
- Minor, W., M. Cymborowski, Z. Otwinowski, and M. Chruszcz. 2006. HKL-3000: the integration of data reduction and structure solution—from diffraction images to an initial model in minutes. *Acta Crystallogr. D Biol. Crystallogr.* 62: 859–866.
- McCoy, A. J., R. W. Grosse-Kunstleve, P. D. Adams, M. D. Winn, L. C. Storoni, and R. J. Read. 2007. Phaser crystallographic software. *J. Appl. Crystallogr.* 40: 658–674.
- Adams, P. D., P. V. Afonine, G. Bunkóczi, V. B. Chen, I. W. Davis, N. Echols, J. J. Headd, L. W. Hung, G. J. Kapral, R. W. Grosse-Kunstleve, et al. 2010. PHENIX: a comprehensive Python-based system for macromolecular structure solution. *Acta Crystallogr. D Biol. Crystallogr.* 66: 213–221.
- DiMaio, F., T. C. Terwilliger, R. J. Read, A. Wlodawer, G. Oberdorfer, U. Wagner, E. Valkov, A. Alon, D. Fass, H. L. Axelrod, et al. 2011. Improved molecular replacement by density- and energy-guided protein structure optimization. *Nature* 473: 540–543.
- Murshudov, G. N., P. Skubák, A. A. Lebedev, N. S. Pannu, R. A. Steiner, R. A. Nicholls, M. D. Winn, F. Long, and A. A. Vagin. 2011. REFMAC5 for the refinement of macromolecular crystal structures. *Acta Crystallogr. D Biol. Crystallogr.* 67: 355–367.
- Emsley, P., and K. Cowtan. 2004. Coot: model-building tools for molecular graphics. *Acta Crystallogr. D Biol. Crystallogr.* 60: 2126–2132.
- Chen, V. B., W. B. Arendall, III, J. J. Headd, D. A. Keedy, R. M. Immormino, G. J. Kapral, L. W. Murray, J. S. Richardson, and D. C. Richardson. 2010. MolProbity: all-atom structure validation for macromolecular crystallography. *Acta Crystallogr. D Biol. Crystallogr.* 66: 12–21.
- Kastritis, P. L., I. H. Moal, H. Hwang, Z. Weng, P. A. Bates, A. M. Bonvin, and J. Janin. 2011. A structure-based benchmark for protein-protein binding affinity. *Protein Sci.* 20: 482–491.
- Zdanov, A., C. Schalk-Hihi, S. Menon, K. W. Moore, and A. Wlodawer. 1997. Crystal structure of Epstein-Barr virus protein BCRF1, a homolog of cellular interleukin-10. *J. Mol. Biol.* 268: 460–467.
- Kotenko, S. V. 2002. The family of IL-10-related cytokines and their receptors: related, but to what extent? *Cytokine Growth Factor Rev.* 13: 223–240.
- Huang, J., S. V. Smirnov, A. Lewis-Antes, M. Balan, W. Li, S. Tang, G. V. Silke, M. M. Pütz, G. L. Smith, and S. V. Kotenko. 2007. Inhibition of type I and type III interferons by a secreted glycoprotein from Yaba-like disease virus. *Proc. Natl. Acad. Sci. USA* 104: 9822–9827.
- Kotenko, S. V., C. D. Krause, L. S. Izotova, B. P. Pollack, W. Wu, and S. Pestka. 1997. Identification and functional characterization of a second chain of the interleukin-10 receptor complex. *EMBO J.* 16: 5894–5903.
- Pletnev, S., E. Magracheva, S. Kozlov, G. Tobin, S. V. Kotenko, A. Wlodawer, and A. Zdanov. 2003. Characterization of the recombinant extracellular domains of human interleukin-20 receptors and their complexes with interleukin-19 and interleukin-20. *Biochemistry* 42: 12617–12624.
- Mendoza, J. L., W. M. Schneider, H. H. Hoffmann, K. Vercauteren, K. M. Jude, A. Xiong, I. Moraga, T. M. Horton, J. S. Glenn, Y. P. de Jong, et al. 2017. The IFN- λ -IFN- λ R1-IL-10R β complex reveals structural features underlying type III IFN functional plasticity. *Immunity* 46: 379–392.
- Lubkowski, J., F. Hennecke, A. Plückthun, and A. Wlodawer. 1999. Filamentous phage infection: crystal structure of g3p in complex with its coreceptor, the C-terminal domain of TolA. *Structure* 7: 711–722.
- Collaborative Computational Project, Number 4. 1994. The CCP4 suite: programs for protein crystallography. *Acta Crystallogr. D Biol. Crystallogr.* 50: 760–763.
- Gromiha, M. M., and K. Yugandhar. 2017. Integrating computational methods and experimental data for understanding the recognition mechanism and binding affinity of protein-protein complexes. *Prog. Biophys. Mol. Biol.* 128: 33–38.
- Soo, C., W. W. Shaw, E. Freymiller, M. T. Longaker, C. N. Bertolami, R. Chiu, A. Tieu, and K. Ting. 1999. Cutaneous rat wounds express c49a, a novel gene with homology to the human melanoma differentiation associated gene, mda-7. *J. Cell. Biochem.* 74: 1–10.
- Wang, M., Z. Tan, R. Zhang, S. V. Kotenko, and P. Liang. 2002. Interleukin 24 (MDA-7/MOB-5) signals through two heterodimeric receptors, IL-22R1/IL-20R2 and IL-20R1/IL-20R2. *J. Biol. Chem.* 277: 7341–7347.